LOW-COST FLUORESCENCE SENSOR FOR ACCURATE DETECTION OF PH VALUE

by

Zachary Splain

BSEE, Rochester Institute of Technology, 2009

Submitted to the Graduate Faculty of

Swanson School of Engineering in partial fulfillment

of the requirements for the degree of

Master of Science in Electrical Engineering

University of Pittsburgh

2015

UNIVERSITY OF PITTSBURGH

SWANSON SCHOOL OF ENGINEERING

This thesis was presented

by

Zachary Splain

It was defended on

August 31, 2015

and approved by

Zhi-Hong Mao, Ph.D., Associate Professor, Department of Electrical and Computer Engineering

Guangyong Li, Ph.D., Associate Professor, Department of Electrical Engineering

Thesis Advisor: Kevin Chen, Ph.D., Associate Professor, Department of Electrical and Computer Engineering

LOW-COST RATIOMETRIC FLUORESCENCE SENSORS FOR ACCURATE DETECTION OF PH VALUE

Zachary Splain, M.S.

University of Pittsburgh, 2015

Fluorometric sensing is a major optical measurement approach widely used in chemical, biological, and medical fields. In conventional fluorescence measurements, two approaches have been used to build low-cost fluorescence sensors. The first approach is to use CCD detector arrays, which incur low sensitivity. The second approach is to use a narrow bandpass filter, which incur low selectivity.

In this thesis, a low-cost ratiometric fluorescence sensor was developed to achieve high sensitivity and high selectivity simultaneously. Two highly sensitive photodetectors were used to monitor fluorescence signal excited by two ultraviolet LEDs with different emitting wavelengths to achieve the sensitivity close to single photon counting. The ratio of fluorescence signals excited by two LEDs was used to identify targeted species with improved selectivity.

This thesis describe the design, development, implementation of optical components, mechanic housing, digital and analog circuits that enable the ratiometric fluorescence measurements. The applications and functionalities of the sensor was demonstrated to measure pH values in liquid solution. The low-cost sensing systems can be programmed in stand-alone operation or be controlled by a laptop or a cellular devices for a wide spread applications including water quality monitoring, biological sensing, and chemical processing monitoring.

TABLE OF CONTENTS

LIST OF TABLES

LIST OF FIGURES

PREFACE

The following sections in this paper utilize many different acronyms and abbreviations. The following table forms a concise list of all of the acronyms and abbreviations used in the paper and provides a clear definition for all of them. Some abbreviations found in the paper will be locally defined.

Table 1: Acronyms and Abbreviations

I^2C	**I**nter-**I**ntegrated **C**ircuit
SPI	**S**erial **P**eripheral **I**nterface
UART	**U**niversal **A**synchronous **R**eceiver/**T**ransmitter
LDO	**L**ow-**D**ropout **R**egulator
TVS	**T**ransient **V**oltage **S**uppressor
GPIO	**G**eneral **P**urpose **I**nput / **O**utput
LED	**L**ight **E**mitting **D**iode
CCD	**C**harge-**C**oupled **D**evice
UV	**U**ltra**v**iolet
USB	**U**niversal **S**erial **B**us
PCB	**P**rinted **C**ircuit **B**oard
EMI	**E**lectro**m**agnetic **I**nterference
IC	**I**ntegrated **C**ircuit
ESD	**E**lectro**s**tatic **D**ischarge
HASL	**H**ot **A**ir **S**older **L**eveling
PCA	**P**rinted **C**ircuit **A**ssembly
RoHS	**R**estriction **o**f **H**azardous **S**ubstances
SRAM	**S**tatic **R**andom **A**ccess **M**emory
MOSFET	**M**etal **O**xide **S**emiconductor **F**ield **E**ffect **T**ransistor
NTC	**N**egative **T**emperature **C**oefficient
TIA	**T**rans**i**mpedance **A**mplifier
ADC	**A**nalog to **D**igital **C**onverter
PGA	**P**rogrammable **G**ain **A**mplifier
RF	**R**adio **F**requency
DI	**D**e**i**onized
HCL	**H**ydrogen **C**h**l**oride

1.0 INTRODUCTION

1.1 FLUORESCENCE SPECTROSCOPY

Fluorescence spectroscopy measures the intensity of the emitted photons from a sample after said sample has been excited by an external light source. Fluorescence is the photon emission process that occurs as a result of a molecule that relaxes from an electronically excited state [1]. To facilitate the change in energy states, the molecules must first undergo excitation which is accomplished by using an external excitation source (light). Once the external excitation is removed, the molecules will begin to relax and return to their ground states [1]. During this relaxation, photons are emitted and the corresponded emitted photons are sensed by a fluorometer [1]. Typically, fluorometers use a broadband light source with relatively uniform intensity (i.e. xenon arc lamps). The excitation source is oriented perpendicular to the detection path to reduce the effect of the excitation source bleeding over into the detection path. The detector for these devices are highly sensitive and are typically CCD (charge-coupled devices) or photomultipliers [1]. The following figure represents a typical fluorometer device.

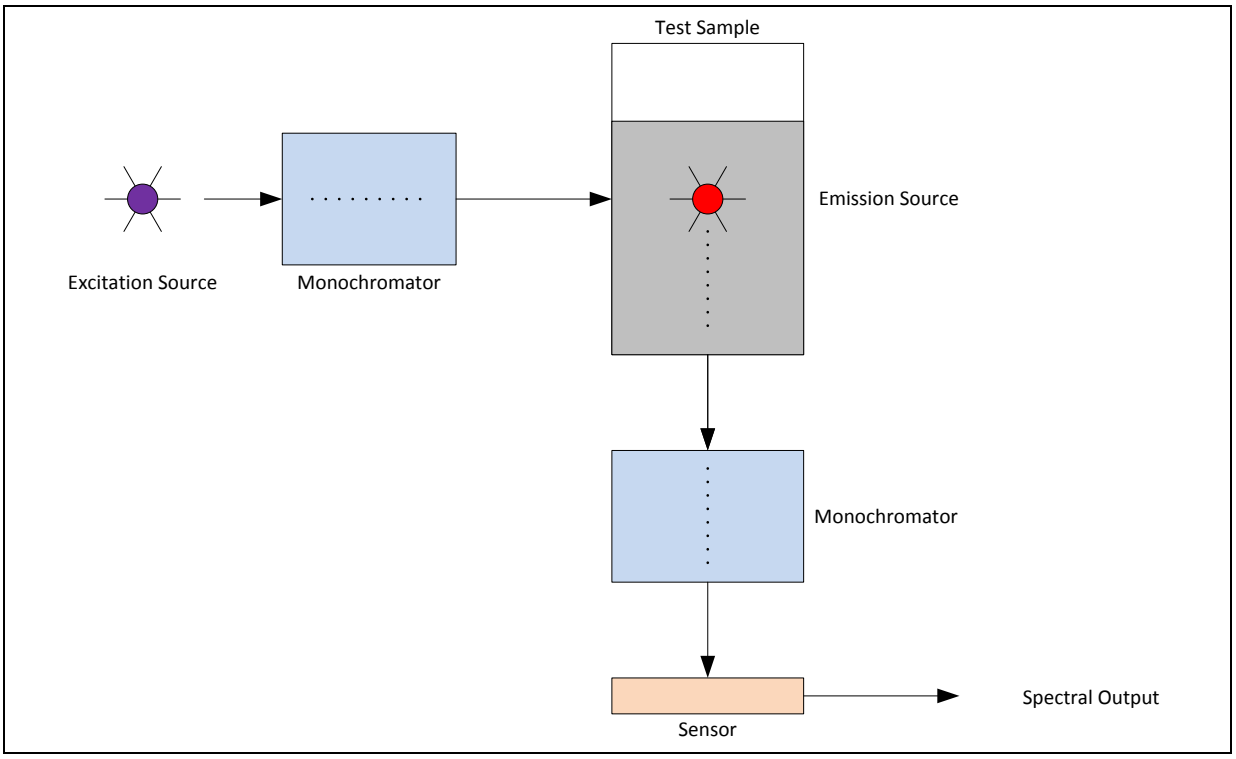

Figure 1: Typical Fluorescence Spectroscopy Setup

The monochromators on both the excitation and emission sides can be turned independently to allow for high resolution / high selectivity of a fluorescence measurement. This allows for highly accurate analysis but this device can be extremely costly and bulky. This type of system does not lend itself to use in remote applications due to its size. Additionally, multi-site monitoring of fluorescence is not feasible due to the high cost associated with this type of device.

1.2 SINGLE COLOR FLUORESCENCE SENSOR

High sensitivity spectrometers tend to be bulky and expensive. For this reason, it is common practice for a single color fluorescence sensor to be used. The principle operation behind this configuration is a narrow band light source (i.e. UV laser or UV LED with narrow band pass

filter) is used to provide the excitation to the test sample. The test sample will fluoresce (emit light at another wavelength) for which, a narrow band pass filter will be used to acquire the single fluoresced color. The following figure (Figure 2) represents a typical setup using this type of architecture.

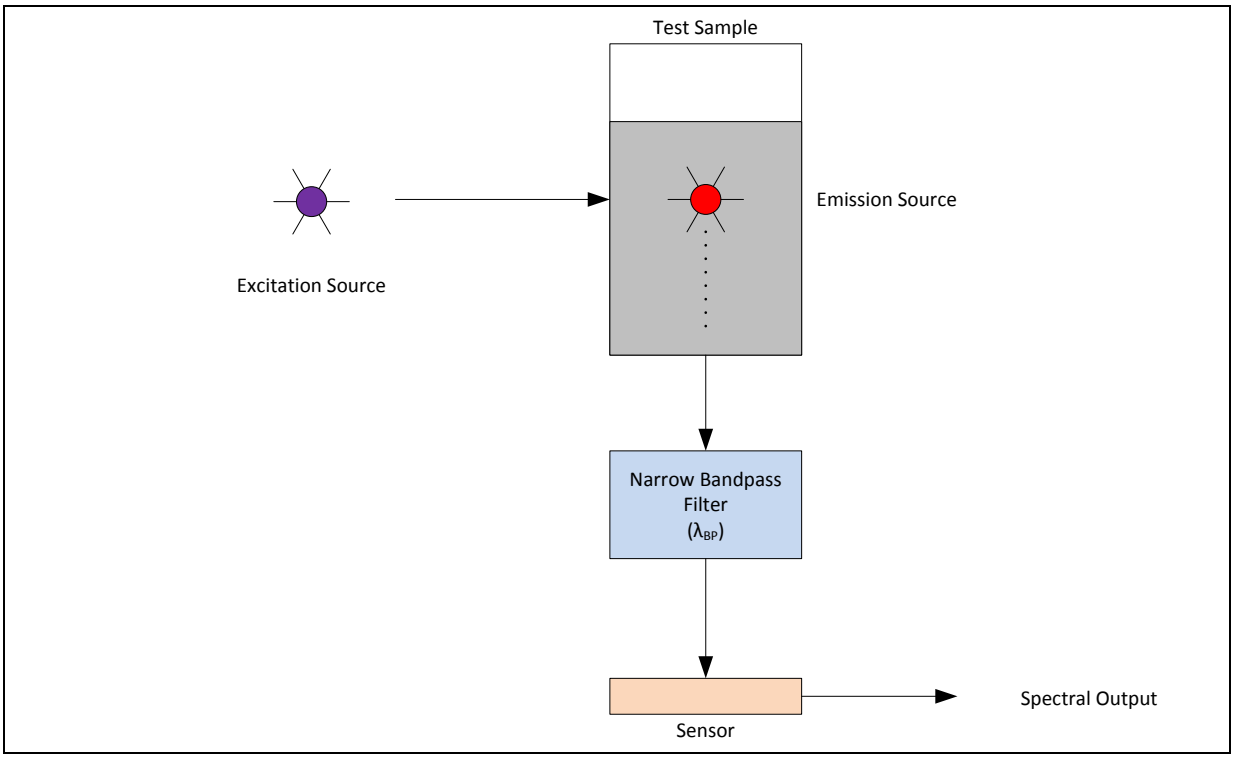

Figure 2: Single Color Fluorometer Setup

This sensing architecture is advantageous because it can be implemented with minimal components at a reasonable cost level; however, the system performance can greatly be affected by background fluorescence. It is common for there to be background fluorescence in a test environment and if background fluorescence is present and happens to be in band of the narrow band pass filter then the measured results will be inaccurate.

1.3 RATIOMETRIC FLUORESCENCE SENSOR

A further advancement in fluorescence sensing utilizes an approach known as ratiometric sensing. There are many different types of materials that fluoresce at the same wavelength which tends to add noise and uncertainty to a measurement. Instead of looking at the intensity of the fluorescence (which is the principle in other measuring techniques) this approach looks at the relative ratio between two measurements. There are two principle ways of implementing this type of sensor. The first is illustrated in Figure 3 below. As can be seen, a test sample is excited with two different sources denoted as excitation source 1, corresponding to wavelength of λ_1 and excitation source 2, corresponding to wavelength of λ_2. The emitted light from the test sample is filtered using a narrowband, band pass filter with the passband center wavelength denoted by λ_{BP}. The concept here is that different samples will fluoresce at differently wavelengths depending on the excitation source.

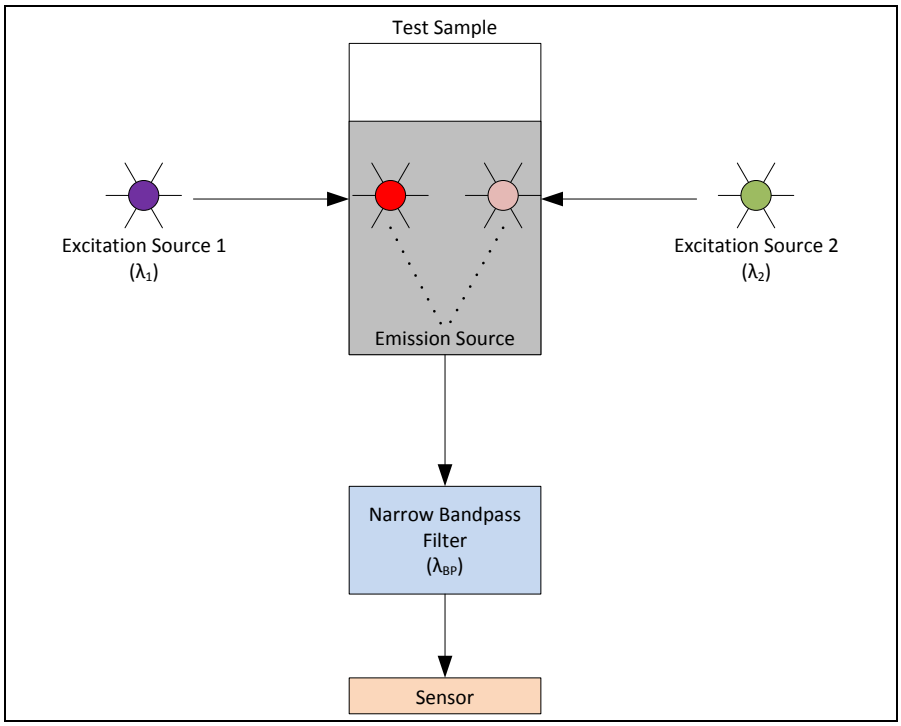

Figure 3: Ratiometric Fluorescence Sensing using Two Excitation Sources and a Narrow Band Filter (sample configuration)

Another approach to implementing a ratiometric sensing system is to utilize a single excitation source and sensing two distinct wavelengths. This approach is illustrated in the following figure, Figure 4. As shown, a single excitation source is used but in contrast to the other configuration, the emitted light is passed through two separate filters which provides a fluorescence measurement with a controlled sensing mechanism.

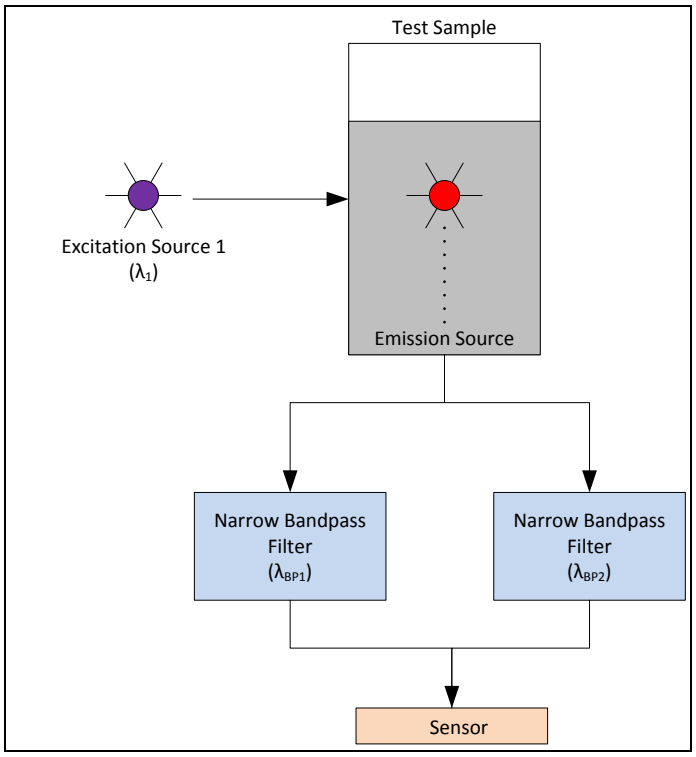

Figure 4: Ratiometric Sensing using Single Excitation Source (sample configuration)

Both configurations provide a means of ratiometric sensing and perform similar to each another. In either configuration it is common to use two distinct fluorescent dyes with two peaks in either their emission or excitation spectrum [2]. In any case, the ratiometric approach has many added benefits over the more conventional steady-state versions [2]. The more conventional steady-state devices are prone to optical path losses, photo bleaching, scattering and background light which requires both recalibration of the instrument and a highly controlled testing environment [2].

Due to climate change and the overall globally warming phenomenon, the concentration of CO_2 has risen which has led to a change in the overall pH level of today's ocean. The oceans are becoming more and more acidic which is having an adverse effect on the biological ecosystems. It has become increasing more important to monitor the changes in the ocean acidification in order to help mitigate the long term effects and potentially validate changes being made across the world to help curb CO_2 emissions. The development of a low cost sensor that can

be deployed in remote areas can be a powerful tool for monitoring the changes in the oceans pH. There is a paper that discusses the development of a low cost fluorescence sensor used to detect the level of pCO_2 (partial pressure CO_2) in the ocean. Here they have used a ratiometric architecture that can be produced for less than $1000 dollars which is relatively cheap given all of the options currently on the market [3]. Their system utilizes a blue and violet LED as a dual excitation [3]. Their approach uses a dichroic mirror and a beam combiner which contains a 90/10 splitter for which 10% of the excitation light is directed towards a reference photodiode [3]. This added photodiode reference is used to normalize the detected fluorescence intensity [3]. By incorporating this reference diode, the effects of temperature and long-term drift of the sensor are minimized [3]. Experimentally the sensor tested to have an average resolution of 1.7uatm [3].

In addition to sensing pCO_2 levels ratiometric fluorescence sensors have gained popularity in measuring pH, Ca^{2+}, Mg^{2+}, Zn^{2+} and heavy metals [2]. The fluorescence dyes used when in contact with a particulate analyte change the amplitude of the peak of its emission which can be used to detect various concentration levels depending on the amount of change in the detected peak [2]. This is the basic principle behind the ratiometric sensing; as the peaks change as a function of the concentration levels of a particular substance, then the detected values will scale ratiometrically. In this paper, the objective was to perform accurate fluorescence measurements with a low cost device. The device is comprised of all solid-state electronics and uses LEDs for an excitation source. The system developed here uses dual excitation sources with each excitation source selected based on the dye to be used. For this case, a 470nm peak blue LED and a 520nm green peak LED were used as the excitation source. Since the LEDs spectral content is considered narrow compared to broadband filament light sources, filters could be used instead of monochromators. The excitation filters chosen were narrow band (10nm bandwidth) filters. This

device was designed to be used with a standard 1cm cuvette which allowed for the optical path to be minimized to reduce path loss [2]. This sensor operates by modulating the LED current to the device at a 3 kHz rate. Each of the LEDs is driven separately and are controlled through switches that are triggered based on the use of a comparator [2]. Each excitation LED is assigned a sign (either positive or negative), if the sign is positive the integrator output voltage is incremented until it reaches the trip point of the comparator for which the other LED is enabled and the sign is flipped (made negative) [2]. At this point, the integrator is then fed a negative voltage and slowly decreases the output of the integrator until it again reaches another trip point [2]. From this point, the LEDs will continue to toggle back and forth. The final output of the device consists of a square wave with varying time intervals that relate to the time excited by a specific excitation source [2]. The ratio of the time intervals is proportional to the luminescence intensity ratio [2]. The period of this square wave is proportion to the concentration of the fluorophore [2]. This device was tested to perform pH readings with accuracy of 0.05pH units [2].

1.4 PROBLEM STATEMENT

The motivation behind this paper is to detail a low cost highly sensitive pH monitoring device. Due to the cost of other technologies and the relative bulky size, the deployment of multiple sensors has been limited. Having low-cost sensors that are able to maintain a high-level of accuracy and sensitivity brings about many advantages. Some of the advantages include: deployment in remote and often harsh environments, analysis can be done onsite, and results can be obtained instantly.

The device in this paper is able to support up to three colors (three analog boards). The following table represents an approximate cost breakdown to construct enough analog and digital boards to produce a single sensor. The total cost for the PCA components is less than $200 but this does not include any overhead for PCA manufacturing since the prototype build of the detector was hand assembled.

Table 2: Component Cost Breakdown

Item	Price	Notes
Digital Board Components	$ 52.74	Parts valued at 1k purchase quantity
Analog Board Components	$ 30.43	Parts valued at 1k purchase quantity
Digital / Analog Board PCB Panel	$ 49.03	50 piece quantity at 1 week turn (each panel contains 3 analog and 1 digital)
Optical Filters	$ 180.00	Estimated price each (6 needed per complete assembly)
Device Total	**$ 1273**	3 analog boards, 1 digital board, 6 optical filters

2.0 SYSTEM DESIGN

This chapter dives into the design of the fluorescence detector. To ensure high-sensitivity and low-noise detection, the analog and digital circuits are separated onto two boards. The digital circuit board allows for the control of up to three analog boards and to facilitated simultaneous measurements of up to three fluorescence sensors. Each of the analog boards contains its own excitation LED light source / filter and high-sensitivity detection circuit to monitor a specific fluoresced wavelength to ensure specificity and selectivity. By controlling the sensors data acquisition time sequence, the device is able to perform flexible ratiometric fluorescence measurements.

The digital board technology is based on the Arduino Mega platform that has been adapted to fit this specific purpose. The Arduino platform is able to reduce the time required for code development due to the availability of many non-standard C++ library functions that have already been created. Furthermore, the Atmel MEGA family of processors has adequate flash space for the application code, computational power and appropriate sampling rate.

2.1 DIGITAL DESIGN AND IMPLEMENTATION

The digital board system level block diagram is shown in Figure 5 below. This shows the entire system hierarchy and communication protocols used to interface with each of the sub-components that are used to build the entire digital board.

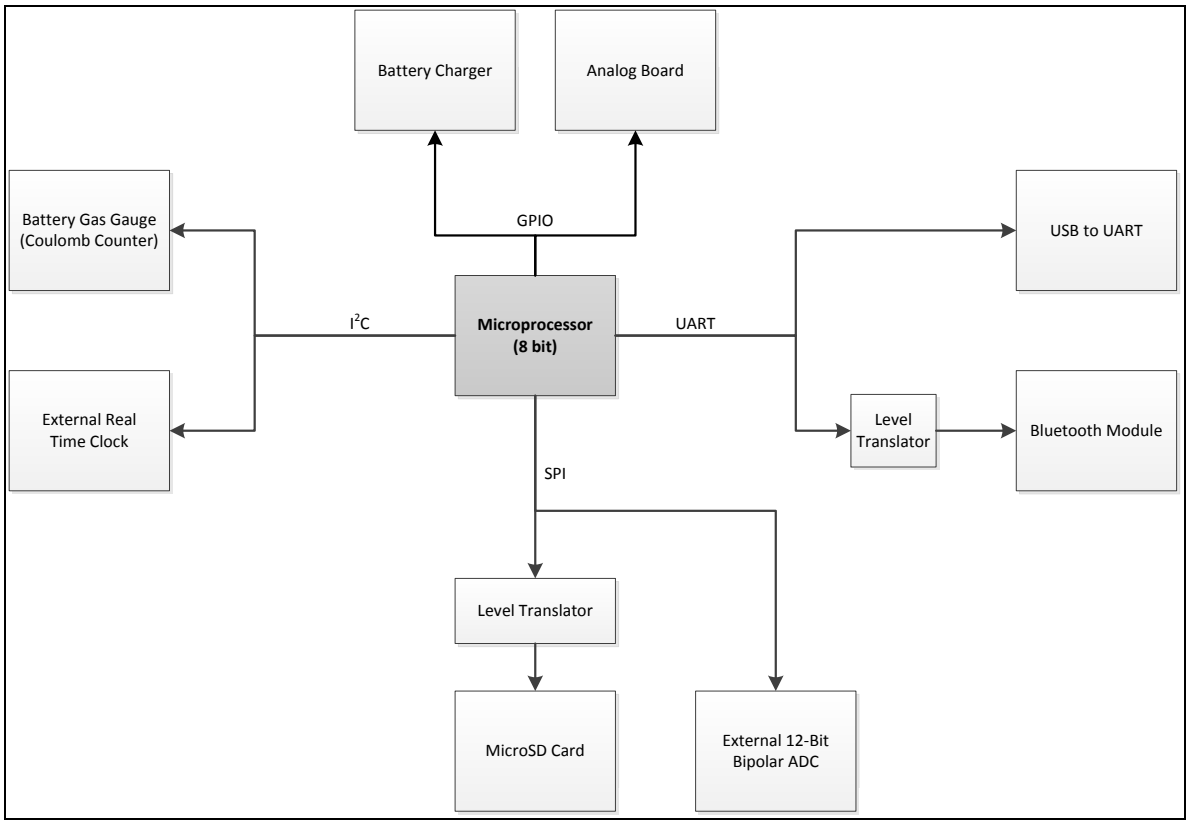

Figure 5: Digital Board System Block Diagram

From Figure 5, the following table (Table 3) highlights the components used and what their primary functions are.

Table 3: Digital Board System Component Identification

Functional Unit	Component Used	Primary Function
Micro-processor	Atmel ATMEGA2560	Brain of the board, used to control all auxiliary units and process the data.

Table 3 (continued)

Functional Unit	Component Used	Primary Function
Analog-to-Digital Converter (ADC)	Texas Instruments ADS8638	SPI interfaced, ADC which allowed for true bipolar measurements. Used to sample analog board data.
Li-Ion Charger	Linear Technology LTC4053	Used to charge the batteries while connected to the USB bus voltage.
Boost Converter	Linear Technology LT1935	Used to boost up the source voltage (either battery or USB bus voltage)
Low-Dropout Regulators (LDO)	Texas Instruments TPS73501	Used to down regulate the boost voltage to provide stable power rails. High current capable.
Inverting Charge Pump	Linear Technology LTC1983-5	Used to provide a -5V power rail for the use in the bipolar analog sensing.
Bluetooth Module	HC-05	Off the shelf Bluetooth module with integrated printed antenna. Used to provide Bluetooth connectivity. Configured using UART communication via the micro-processor.
USB-to-Serial Converter	FTDI FT232R	Used to convert USB data to serial data for communication with the processor.
microSD Level Shifter	Texas Instruments TXB0104	Converts 5V logic to 3.3V logic for the SPI control lines. This is necessary in order to allow the processor and microSD card to communicate.
Bluetooth Level Shifter	Texas Instruments TXS0102	Converts 5V logic to 3.3V logic for the UART control lines. This is necessary in order to allow the processor and the Bluetooth module to communicate.
Battery Gas Gauge	Linear Technology LTC2942	Communications to the processor via I^2C and is used as a means to monitor the battery life remaining.
Real Time Clock (RTC)	Intersil ISL1208	Used to provide the date and time stamp for the data collection. Communicates to the processor via I^2C. Runs off a coin cell battery for continuous time keeping.

Due to the high sensitivity of the analog circuity it was imperative that the digital power be separate from the analog power. To accomplish this the source voltage (either lithium ion battery or USB bus power) is boosted up to approximately +6V and post-regulated back down the

desire rail voltages. For the digital hardware on the board, both a +3.3V supply rail and a $+5V_{DIG}$ supply rail were necessary due to some of the integrated circuits not being +5V tolerant. The analog board (discussed in detail in a subsequent section) requires a symmetric bipolar supply. This was accomplished by regulating down the boost voltage to the $+5V_{ANA}$ power rail which in turn was inverted using an inverting charge pump regulator to generated the $-5V_{ANA}$ power rail. The following image is representative of the system power distribution and highlights how each supply voltage is generated.

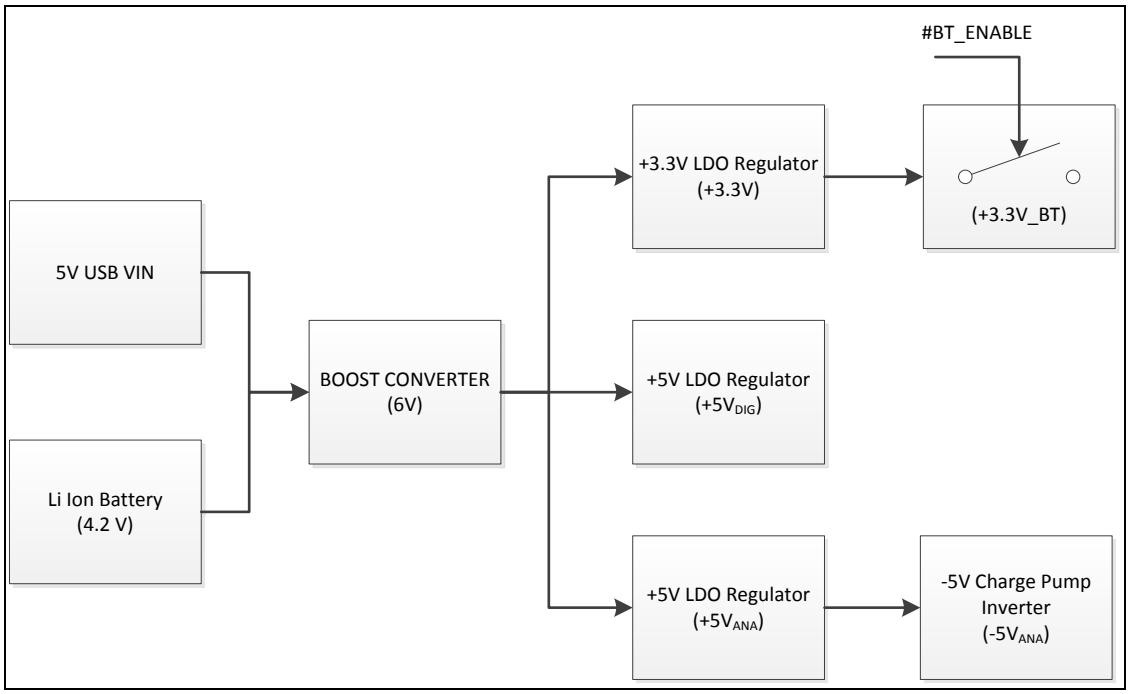

Figure 6: System Power Distribution Network

Special consideration is given to the initial supply generation by sequentially soft-starting during powered up. Some of the IC's used on the board have substantial inrush currents which can prevent the boost circuit from starting up or allow it to enter a latch-up condition. In any case, by staggering the turn on of each power rail, the effects of the initial inrush are minimized. All of the power rails are sequentially enabled with the exception of the $-5V_{ANA}$ supply rail. During initial testing of the

circuit, the -5V_{ANA} rail failed to startup when enabled after the +5V_{ANA} rail. To correct this issue, the -5V_{ANA} rail is enabled as the +5V_{ANA} becomes enabled. The purpose for sequentially soft-starting all of the power rails is to limit the inrush current during startup by allowing each power rail to stabilize before another one is powered on. Soft-starting is accomplished by using a simple RC network on the enable lines of the LDOs and the switching boost regulator. Figure 7 below illustrates the timing for the power-up sequence. One thing to note is that the -5V_{ANA} rail comes on last and this only experiences a small delay due to the output of the +5V_{ANA} power rail coming up. The enable line for the charge pump inverter is tied directly to the input of the charge pump (coincidentally this is the output of the +5V_{ANA} LDO).

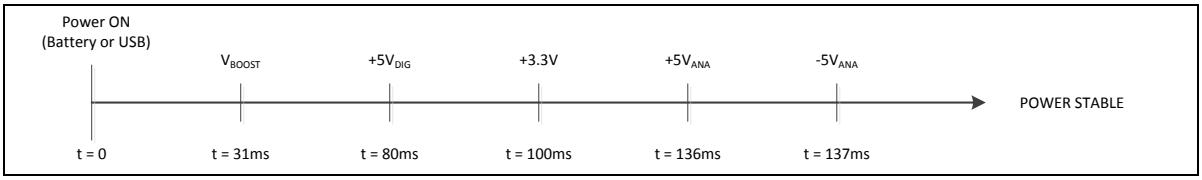

Figure 7: Power-Up Sequencing Timing Diagram

To help reduce the switching noise of the boost regulator each of the low dropout regulators outputs are filtered using a LC Pi-network where the inductor is replaced with a ferrite to provide additional high frequency filtering. Furthermore an RC snubber circuit is connected to the output of the switching node of the boost regulator to provide a means to reduce the overshoot during boost regulation. The current design does not utilize the snubber circuit components since the ripple overshoot during regulation is negligible and does not impact the circuit downstream due to the efficient layout of the circuit on the PCB, the loop inductance is minimized.

The digital board uses several different communication protocols which have various transmit speeds. Some of the communication protocols run at speeds up to 8 MHz so at the source of each transmit, receive, or clock line a series resistor is added to minimize any reflections due to

the edge rate of the digital signals. This is not as much of a concern, however; for commercialization it is imperative that attempts are made to help reduce EMI radiation as this can cause issues with surrounding equipment. For the USB differential traces (D^+ and D^- lines), the routing of these signals is critical so the lengths of each of the differential signal are kept to within 5 decimal places of each other (unit: mm) in order to keep the impedance mismatch to a minimum. For the I^2C, SPI and UART communication lines, preferential routing of these signals on the internal signals layers was maintained.

The digital board utilizes an integrated Bluetooth radio module for all Bluetooth communication. It communicates to the processor via UART bus and is powered down by default in order to minimize battery usage due to the modules high power consumption. The module's power is controlled by an external MOSFET which can be enabled by the processor when Bluetooth operation is required.

The circuit includes a lithium ion battery charger capable of charging a single 4.2V cell. For this detector design, there are two battery connections on the board which will allow for up to 2-battery packs to be used (parallel connection) to provide additional capacity for longer run times for mobile use of the detector. The charging IC is designed to charge the cells at a specific charging rate depending on the status of the USB. If the USB device is not enumerated and is not in sleep mode then the device will charge the cells at 100mA; however, if the device is either enumerated or on a dedicated charging port then the charge current is stepped up to 400mA for faster charging. The charging state is toggled by using the GPIO of the USB-to-Serial chip to sense the state of the USB and depending on the state (i.e. enumerated, sleep, etc.) the GPIO will switch in or out additional resistors on the programming current pin of the charging IC. The programming current pin allows the designer to set the program current and for this design the program current is

selected based on the status of the USB. To further enhance battery life and to get as much runtime out of the batteries as possible, a coulomb counter (gas gauge IC) is on the board which is designed to track the capacity of the battery. This IC is designed to send an interrupt to the processor that signifies the charge remaining has dropped below a programmed threshold. The interrupt allows the processor to end any task that is currently running such as the data collection task and data storage. By shutting down the tasks and allowing the device to shutdown gracefully prevents the logged data from being corrupted or incorrect data to be presented to the user. This is not actively being used by the software to control the shutdown of the data acquisition and data saving.

The primary purpose of this sensor is to be used in remote applications and for this reason the system needs to be robust and hardened from abuse by people and the environment. The digital board only exposes a single connection path from the outside environment to the board and this is through the USB port. The conditions and environment for which the sensor is to be used can be variable and thusly can be exposed to ESD strikes. To mitigate this risk, a specially designed TVS array IC for the use on USB lines is used. The purpose of this device is to clamp and dissipate the energy associated with an electrostatic discharge event. If no protection is in place then performance of the device can be greatly affected and worse the board could be subjected to permanent damage. This TVS diode array is ultra-low capacitance to ensure no adverse effects when placed on the data lines of the USB device. This device is placed between the USB connector and the USB to Serial IC. In the event of an ESD strike the energy will be shunted to the upper rail or to ground (depending on the polarity of the ESD event).

2.1.1 Digital Board PCB Layout

The digital board is a 0.062 inch thick, 6-layer board on standard FR4 substrate. There is 1-oz copper on all layers (1.4mils thick) and the finish is a standard lead-free HASL finish. To minimize the physical board size, the component sizes used on the PCA were small enough to still be populated and built by hand. The passive components (resistors, capacitors, etc.) are as small as 0402 and most of the IC packages were selected in a leadless package where possible. The board stack-up is shown in the following figure.

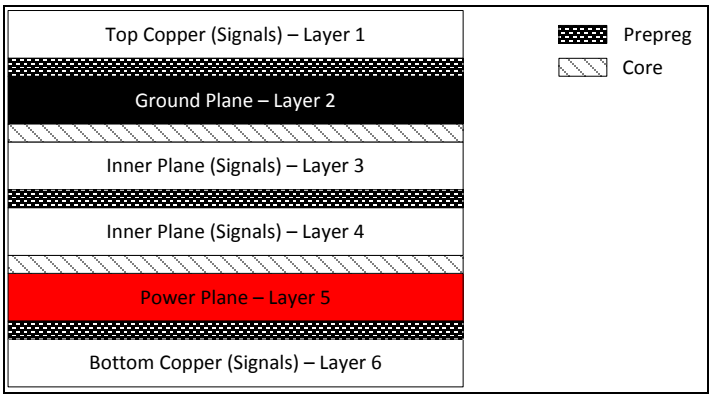

Figure 8: Digital and Analog Board PCA Layer Stack-Up

The inner plane layers were routed perpendicular to each other to reduce crosstalk [4]. Although the signals on this board are not considered highspeed, this technique of routing inner trace layers perpendicular is good practice. Some special considerations were made to layout surrounding the bluetooth module. Since this module contains the bluetooth engine and antenna on the same PCB it was prudent to minimize the copper in the near field of the antenna. The radiation and antenna efficiencies are not known but the tuning of the antenna can be greatly affected by nearby components and any additional metal. The area under and around the printied antenna were kept clear of any copper pours / components /or traces.

The following series of images are layer by layer captures of the digital board. The are viewed top down. The top layer contintins the bluetooth module as well as other ICs (i.e. ADC, real-time clock, etc.). The following image (Figure 9) is the top layer / component layer of the board.

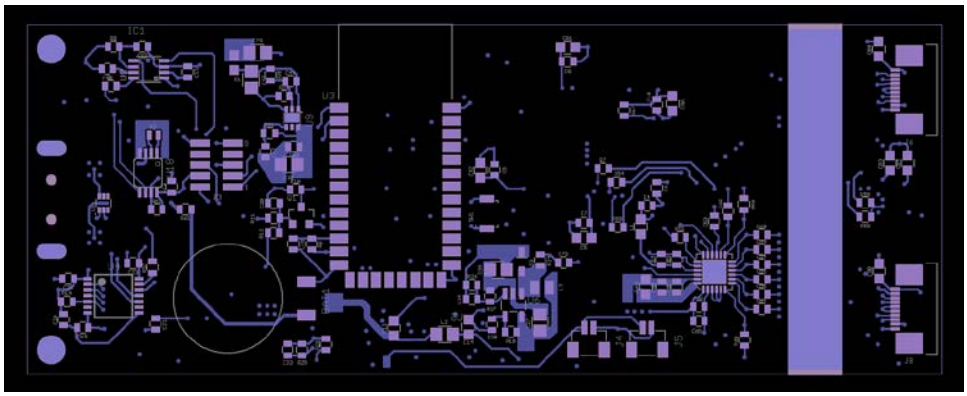

Figure 9: Digital Board Top Copper / Component Layer (layer 1)

Figure 10 below is the ground plane layer of the digital board. It is a solid ground pour of copper with a void under the Bluetooth antenna to help reduce the impact of detuning on the circuit. Since this board is primarily a digital board there was no need to split the ground planes into a digital and analog section; however, the grounds on the analog board are kept split and tied in a single point under the board connector. This will be discussed in greater detail in the analog section.

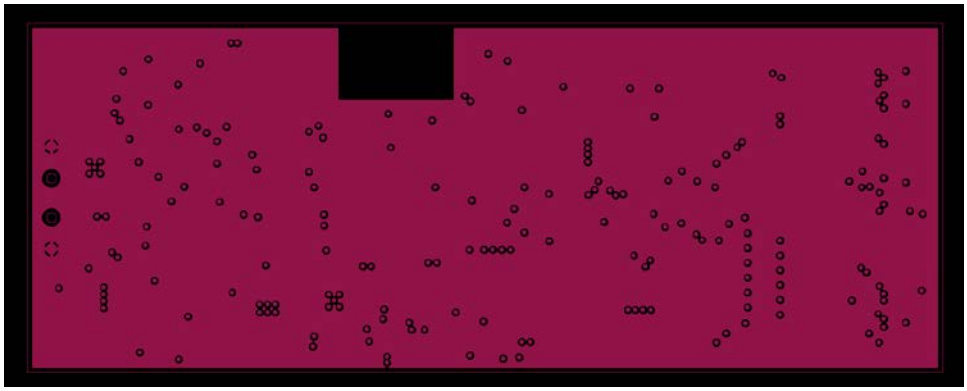

Figure 10: Digital Board Ground Plane (layer 2)

Figure 11 below is the inner layer of the board or layer 3. All of the traces are oriented lengthwise on the board to help reduce crosstalk between the signals on the next layer or layer 4. All of these signals are low speed digital signals (<8MHz).

Figure 11: Digital Board Inner Signal Layer (layer 3)

In contrast to the routing of layer 3, layer 4 shown in Figure 12 are all run perpendicular to layer 3 which is designed to reduce the crosstalk between the adjacent trace layers [4]. Even though the speeds of these digital signals is relatively slow and there is a low risk of crosstalk and issues arising from this, it is just good practice to route traces on adjacent layers perpendicular to each other.

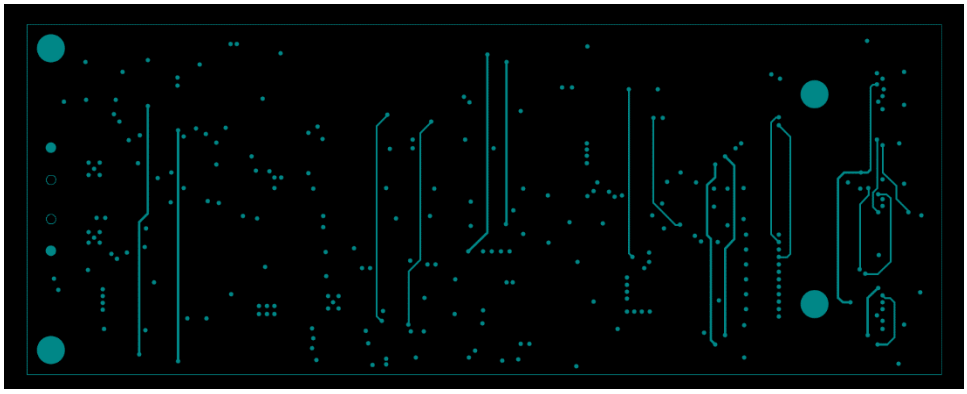

Figure 12: Digital Board Inner Signal Layer (layer 4)

The next layer down is the power plane layer which can be seen in Figure 13 below. All of the power connections are made to this plane through vias from the top and bottom surface. There are several different copper islands which represent different power rails. The point at which the power rails are generated (i.e. the output of an LDO or boost) the power trace is stitched with multiple vias to the power plane to allow for low ohmic power connections and to reduce the inductance introduced by using vias. Multiple vias together act like parallel inductors which consequently lower the overall inductance seen by the power supply. It is also important to note that all high power connections to the power plane are done using multiple vias and thick traces.

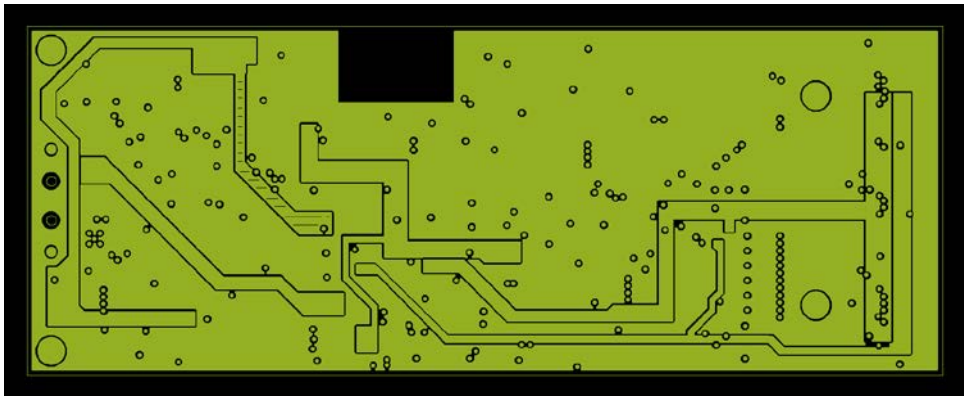

Figure 13: Digital Board Power Plane (layer 5)

The bottom layer consists of additional components and signal traces. This layer contains the processor, USB to Serial, microSD, and supplemental circuits. The following image (Figure 14) is of the bottom layer of the board.

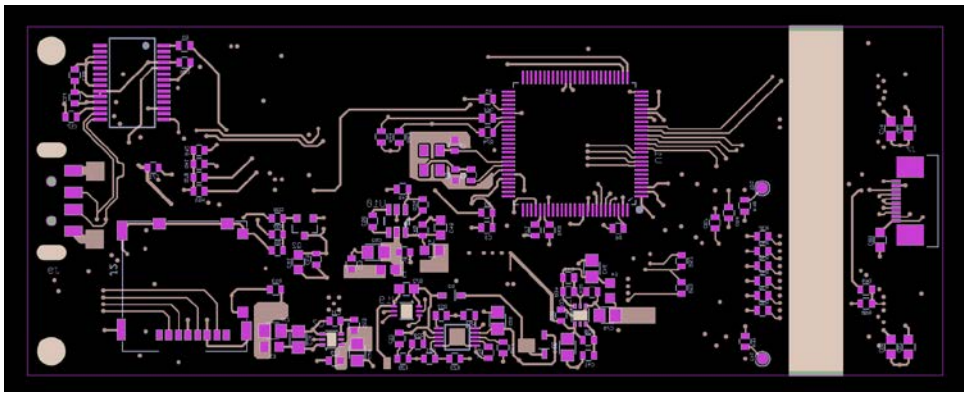

Figure 14: Digital Board Bottom Component Layer (layer 6)

The following figures (Figure 15 and Figure 16) are actual photographs of the complete digital board assembly. This board was assembled by hand using tweezers to place all of the components and solder paste. A single side of the board was assembled and placed into a benchtop reflow oven and then the opposite side of the board was assembled. The process and components selected are RoHS compliant. Each digital board took approximately 6 hours to assembly and test.

Figure 15: Digital Board PCA Front Side, Actual Board

Figure 16: Digital Board PCA Bottom Side, Actual Board

2.2 EMBEDDED SOFTWARE DESIGN

The software for this fluorescence sensor is based on the Arduino (C++) architecture. This device utilizes an 8bit AVR core processor with 256k of flash for program space and 8k of SRAM. The code consists of a main setup loop that is executed upon power up of the processor or during a reset condition. This portion of code is executed exactly once and is used to setup the pin modes (i.e. output, input), SPI bus, I^2C and other functions. After the setup loop has executed, the device enters the main loop which will run continuously until the device is powered off. The main loop is where all of the function calls are executed. The software is based on a custom serial protocol for which all functions are enabled and disabled via a specific string sent to the device over Bluetooth or USB. The following flow chart (Figure 17) represents the code hierarchy.

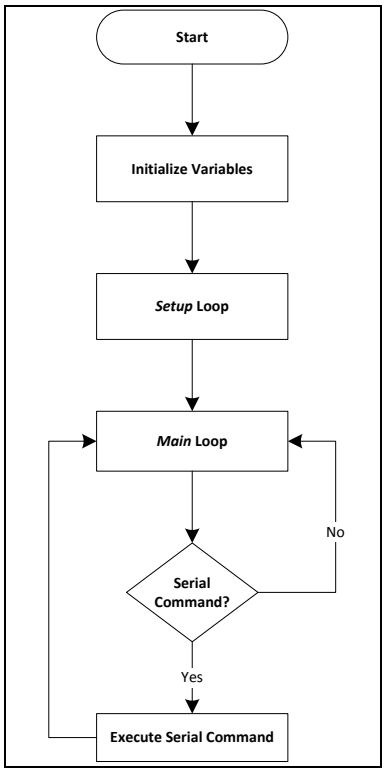

Figure 17: High Level Firmware Architecture

The serial command structure allows for the device to be configured on the fly. All of the function calls that are created are supported via the serial commands. The following figure (Figure 18) represents all of the supported serial commands.

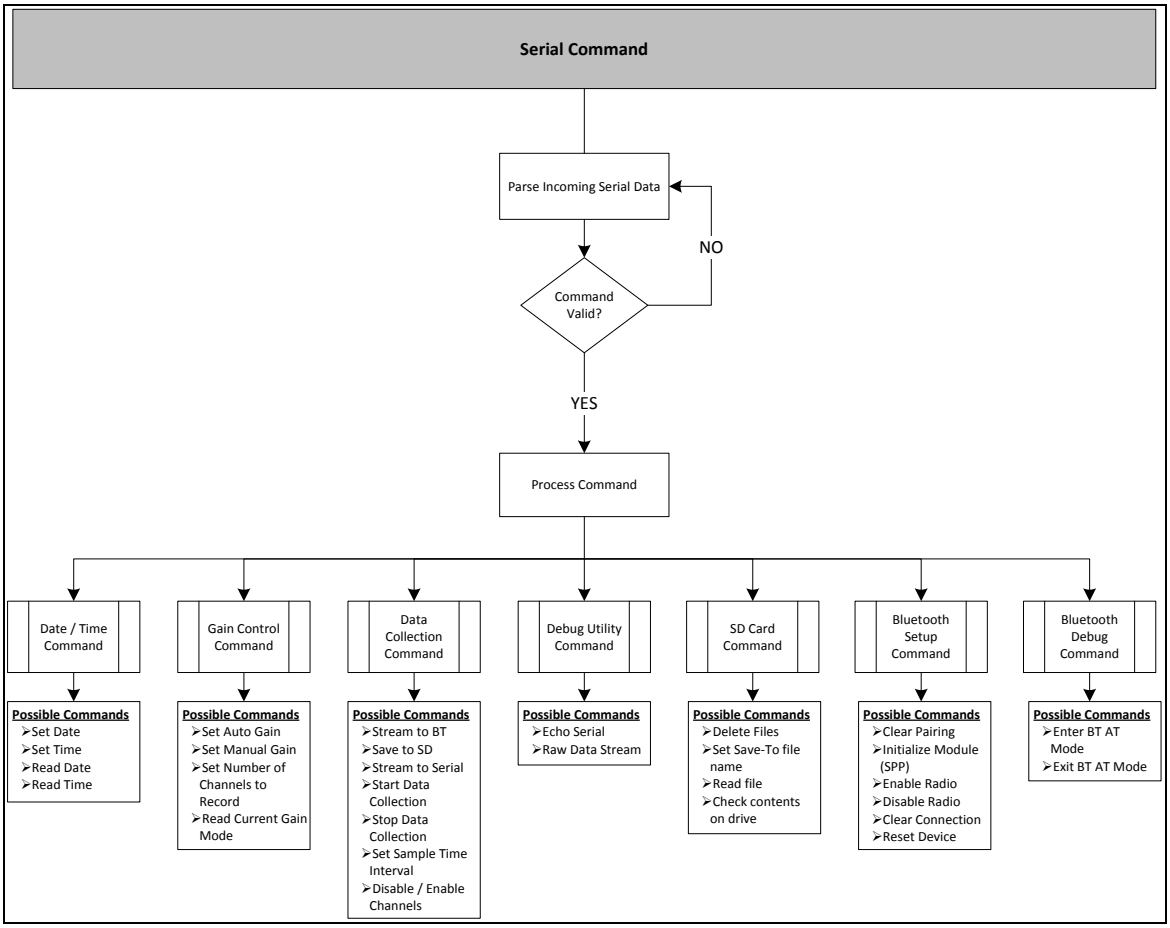

Figure 18: Embedded Software Serial Command Hierarchy

The hardware is designed to support up to three individual sensors, therefore it was vital that the firmware allow for complete configurability. All interfacing with the device is done either using a standard terminal or with a custom LabVIEW application that was created to display the device data and for configuration.

The firmware is responsible for detecting the peak-to-peak voltage of the sampled measurement. To accomplish this the firmware algorithm employs the following software flow (Figure 19).

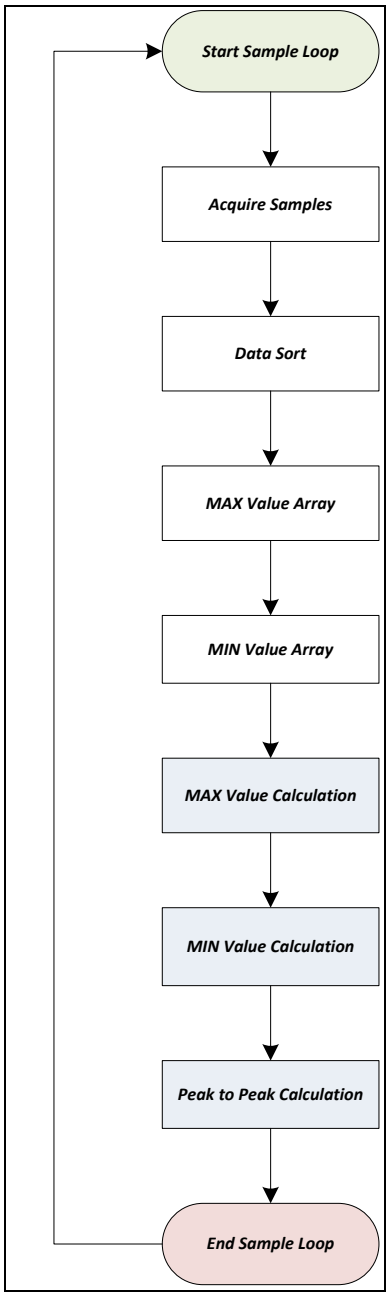

Figure 19: Peak-to-Peak Detection Algorithm

The algorithm samples 100 samples and stores this data into a predefined array. The array undergoes a bubble sort which organizes the sampled data into ascending order. From here two new arrays are created; one being the max value array and the other being the min value array. From the sorted array, the upper 10 values are copied to the max value array (upper 10 values are the largest of the data collected) and the lower 10 values are copied to the min value array (lower

10 values are the smallest of the data collected). To obtain a single max and min value, each of the corresponding arrays is averaged and stored as a single value. The peak-to-peak value is simply the difference between the signal max and the signal minimum thusly, the max and min values are subtracted and the result is the peak-to-peak value for the sampled data. This process repeats itself at a rate selected by the user (by default 2Hz). During sample data loop, the peak-to-peak value is passed to string where it is then either stored to the microSD card or streamed via Bluetooth or serial.

2.3 ANALOG BOARD CIRCUIT DESIGN

The board referred to as the 'analog board' contains all of the sensing circuitry that is used for the fluorescent detector. At a high-level, the following figure (Figure 20) represents the functional blocks of the sensing circuit. The circuit can be split into two sub circuits: 1) LED control circuit and 2) ultra-sensitive fluorescence detection.

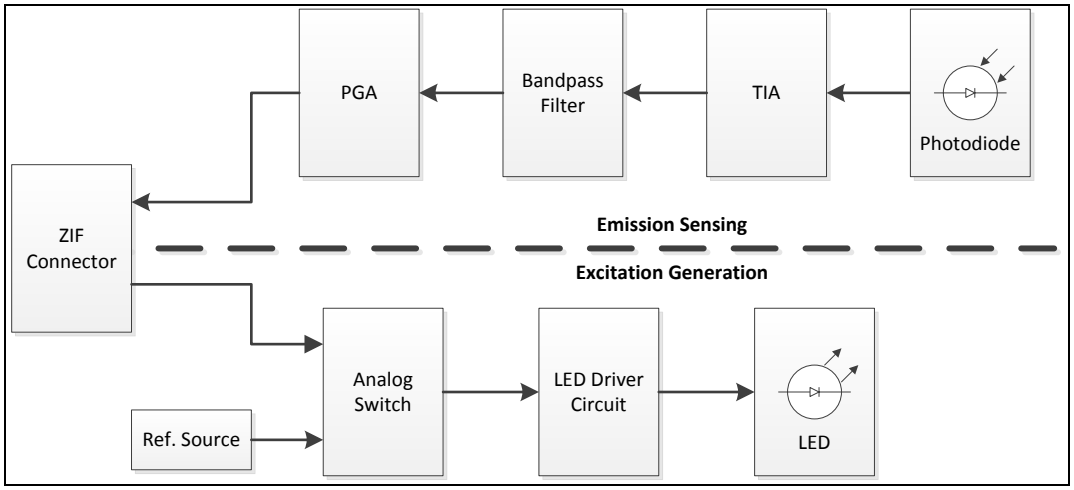

Figure 20: Analog Board High-Level Functional Block Diagram

The control circuit for the LED utilizes a digital output provided by the microprocessor which generates a 1024 Hz pulse train with a 50% duty cycle. The pulse is generated using a built in 16-bit timer in the microprocessor which toggles a GPIO pin. This timer routine uses a standard interrupt routine built into the processor's core library. This pulse train is used to control a power MOSFET to switch on/off the $+5V_{DIG}$ voltage supply to the LED. To limit the LED current, a series resistor is connected to the LED and is sized to provide approximately 5mA of current. This provided enough excitation while minimizing current consumption to help sustain long operation under battery power. Since the LED's performance fluctuates with temperature, a NTC thermistor is mounted near the LED on the analog board. The temperature is recorded as part of a measurement and is stored in the data stream. This temperature reading can be used to compensate for temperature effects as part of the data post processing. The thermistor circuit comprises a resistor divider where the thermistor's change in resistance ultimately changes the output voltage of the resistor divider network.

The design utilizes a transimpedance amplifier to convert the photodetector's current to a corresponding voltage. In order to achieve high sensitivity the circuit is required to be able to convert pico-amps of current to a voltage to be processed by the ADC. This is accomplished by using a high performing TIA and by providing as much isolation as possible from high frequency signals. The output of the TIA is fed into a band pass filter with the passband frequency corresponding to the oscillation frequency of the excitation LED. This was done so that the data being processed corresponds to the fundamental LED pulsing frequency and so that the background noises of analog circuit can be minimized to improve the detection sensitivity. The final stage in the analog circuitry is the PGA with programmable gain settings of 1, 10 and 100. The purpose of this amplifier is to programmatically change the gain based on a specific algorithm

developed in software. The use of the PGA allows the detector to have a larger dynamic range in order to measure the smallest of concentrations without saturating the sensor.

All of the signals on the analog board are bipolar and range from $-5V_{ANA}$ to $5V_{ANA}$. The ADC on the digital board is responsible for taking this bipolar signal and converting it into a digital representation to be processed by the microprocessor. Each sample can be represented by a value ranging from 0 – 4095 (12-bit ADC). This particular ADC can accept true bipolar signals and each sampled channel can be programmed for either bipolar data or unipolar data. The digital output of the ADC can be converted back into a corresponding voltage by taking into account the weight of each digital bit value and scaling it accordingly. This is fundamentally how the device converts the analog signal into a digital signal to be processed.

2.3.1 Analog Board PCB Layout

Similar to that of the digital board, the analog board is also a 6-layer board with the same layer stack-up as shown in Figure 8. The primary difference between these two boards is that the ground plane for this board is split and connected via a 0-ohm resistor under the interfacing connector. Since the analog board consists of highly sensitive analog circuitry and some digital circuitry (LED pulse generation) it was necessary to provide as much isolation between the two grounds. Using a single point connection for the grounds allows the use for an RF choke (if required) to keep the high frequency isolation between the two grounds (but for this current build a zero ohm resistor was installed). The following figure, Figure 21 is the top signal / component layer. The upper portion of the board as viewed contains the analog circuitry while the bottom half contains the digital portion. The highly sensitive transimpendance amplifier circuit is nested within

a guard ring. The guard ring is stitched to the ground plane and helps to reduce the effects of parasitics on the circuit. The outer guard ring was designed such that a copper or metal shield could be soldered around the circuit to act as a faraday cage to prevent or limit the amount of EM interference injected into the TIA. Additionally, the highly sensitive transimpendance input with the photodiode is also encapsulated in a separate guard ring and this is tied to the body pin of the transimpendance amplifier. The body pin is simply the interface to the body of the internal FETs of the IC. The guard rings act to keep surface leakage currents from effecting the sensitive input of the amplifier.

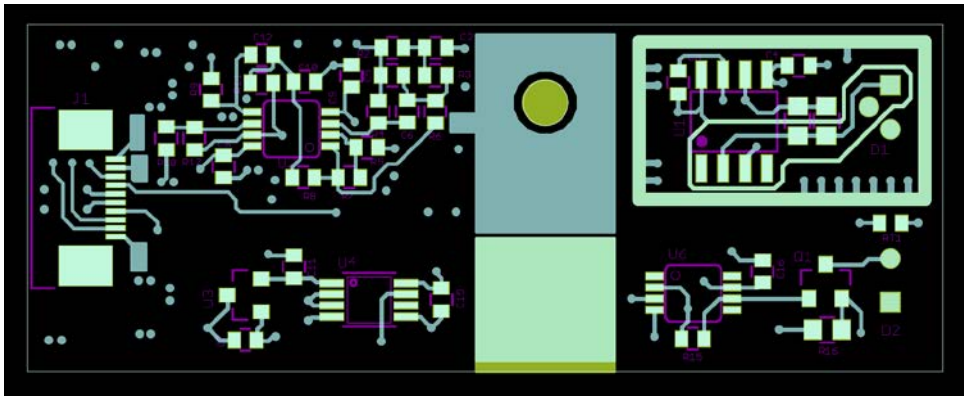

Figure 21: Analog Board Top Copper / Component Layer (layer 1)

The following figure, Figure 22 shows in the internal ground plane of the device. As mentioned before, the ground plane for the analog board is split and connected at a single point to the digital ground at the connector. Since the digital board consist of a single ground, the grounds are combined at the analog connector and fed back to the digital board as a single ground net. Special care was taken to ensure that any mixed signal traces were routed over the ground connection point to ensure that the signal return path to ground was a short as possible. If the signals were routed across the split ground plane then the return path for the ground current would

be large thus reducing the benefit of having two ground planes and potentially adding noise to the circuit.

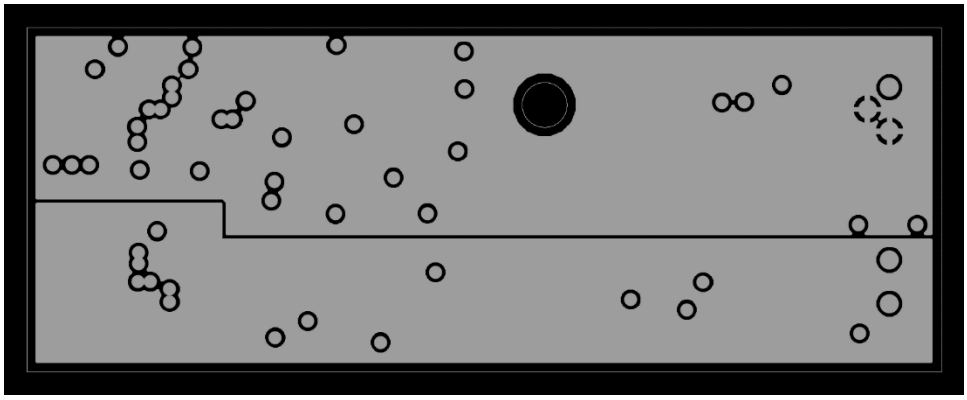

Figure 22: Analog Board Ground Plane (layer 2)

The following two figures, Figure 23 and Figure 24 are the inner signal layers and similar to that of the digital board, care was taken with orientation of the signal routing. Layer 3 was reserved for signal traces to be routed lengthwise of the board whereas layer 4 the traces were routed perpendicular to that of layer 3.

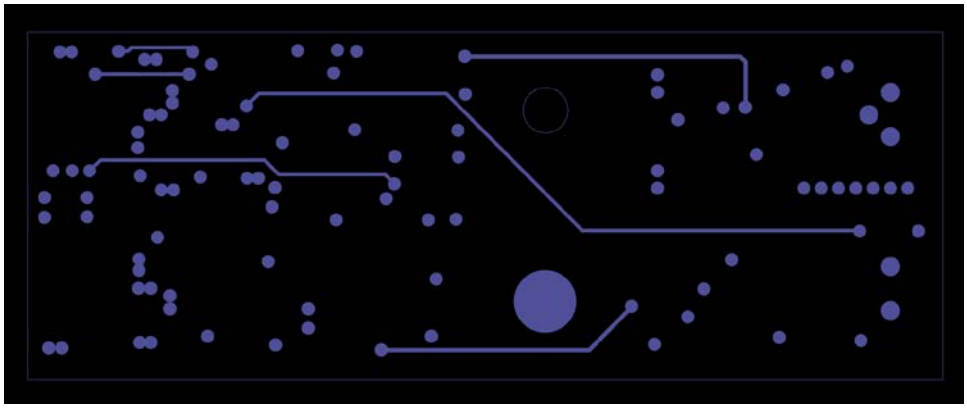

Figure 23: Analog Board Inner Signal Layer (layer 3)

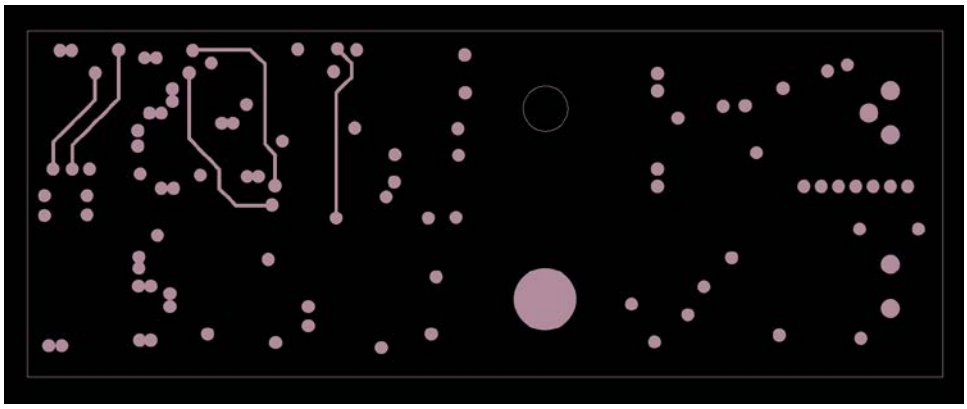

Figure 24: Analog Board Inner Signal Layer (layer 4)

Since the ground plane is split the same is also true for the power plane since there are dedicated power supply rails for the analog and digital circuity. The following figure, Figure 25 shows the power plane or layer 5 of the analog board. It can be seen that the power plane is split and the analog portion (upper half of the board) contains two copper pours one for which is the negative 5V supply rail ($-5V_{ANA}$) and the other is the positive 5V supply rail ($+5V_{ANA}$).

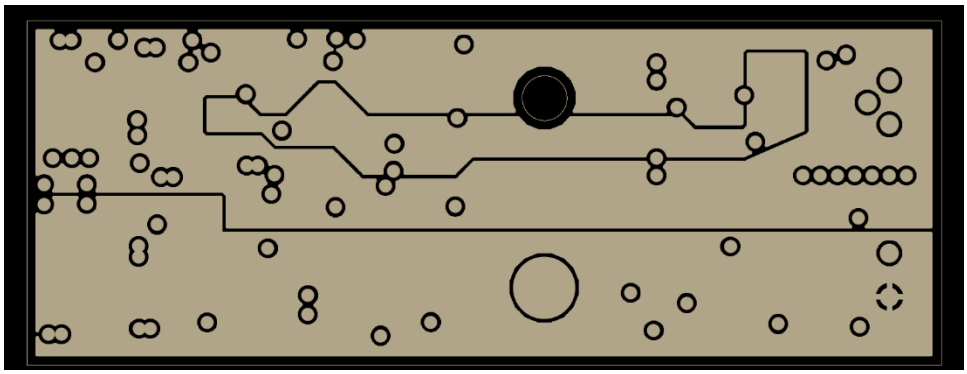

Figure 25: Analog Board Power Plane (layer 5)

Lastly the bottom layer is the bottom copper and component layer. The following figure, Figure 26, shows the layout for the bottom side of the board. For the analog section (upper half of the board) under the sensitive transimpendance circuity there are no traces being routed, instead there is a copper pour that is connected to ground. Again the intent here is to provide additional protection for the transimpendance amplifier.

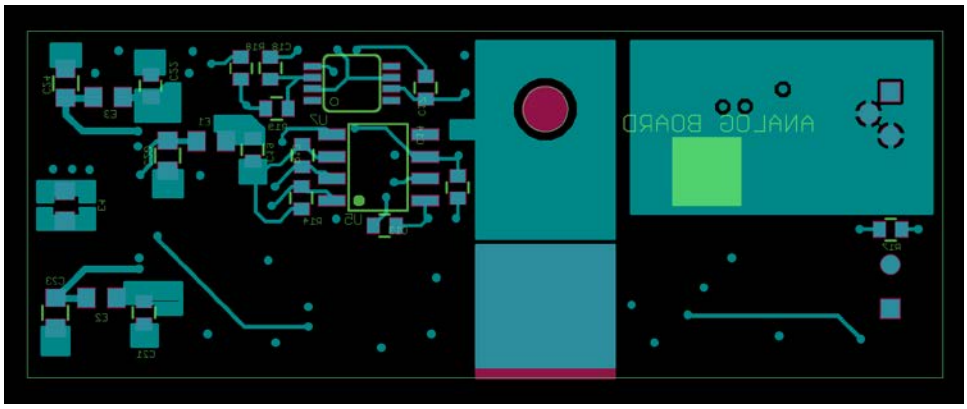

Figure 26: Analog Board Bottom Copper / Component Layer (layer 6)

The following figures (Figure 27 and Figure 28) are actual photographs of the assembled analog PCB both the front side and back side respectfully. The analog boards were assembled in the same manner as that of the digital board. Each analog board took approximately 1 hour to assemble and test.

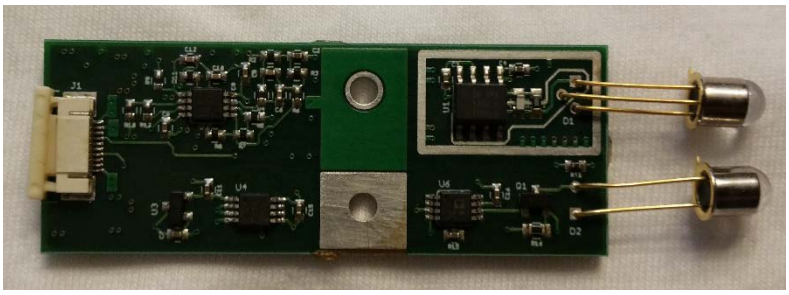

Figure 27: Analog Board Top Side PCA (Physical Photo)

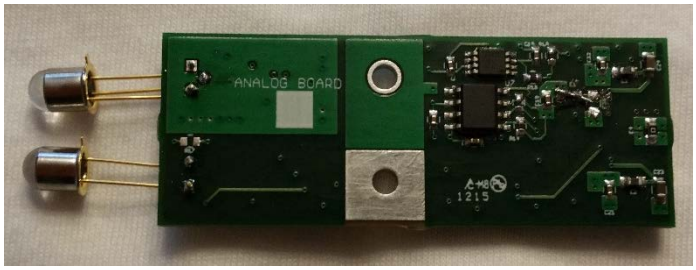

Figure 28: Analog Board Bottom Side PCA (Physical Photo)

3.0 EXPERIMENTAL RESULTS

3.1 ELECTRICAL VERIFICATION TEST

The purpose of this experiment is twofold: 1) signal integrity and 2) electrical performance of the fluorescence detector designed in this paper. To complete this experiment, a common white copy paper is used as a test pattern for the device. A single analog board outfitted with a 310nm excitation filter and 520nm emission filter is installed. The outputs of the TIA, band pass filter stages and the PGA are monitored using a Lecroy Wavesurfer 3054 Oscilloscope. The paper test sheet is placed at various distances from the senor head and the data is recorded using a LabVIEW program developed specifically for this device. The LabVIEW program allows for the device to be configured and for the conversion of the data from the digital board into a usable value. The following image (Figure 29) is representative of the test step-up used.

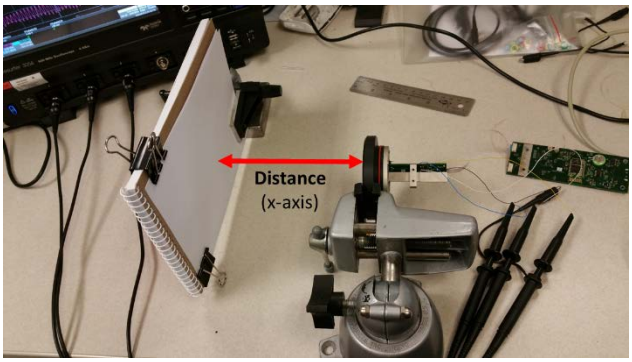

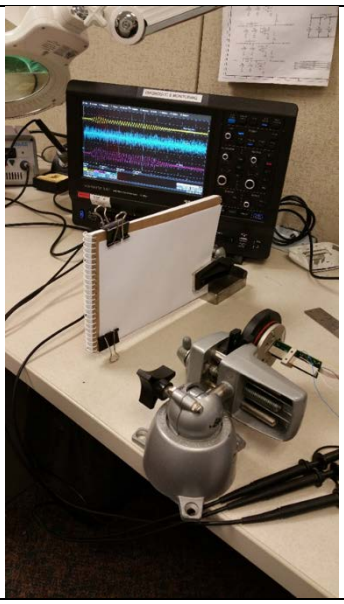

Figure 29: Signal Integrity Test Setup

The device was configured to take a reading every 500msec (2Hz rate). At each position, the data was collected for at least 30 seconds to provide a large sample set for averaging. In Figure 30, the oscilloscope data can be seen for all of the distances tested as part of this experiment. The yellow trace represents the output of the band pass filter stage, the cyan trace represents the output of the transimpedance amplifier, and the magenta trace is the output of the programmable gain array.

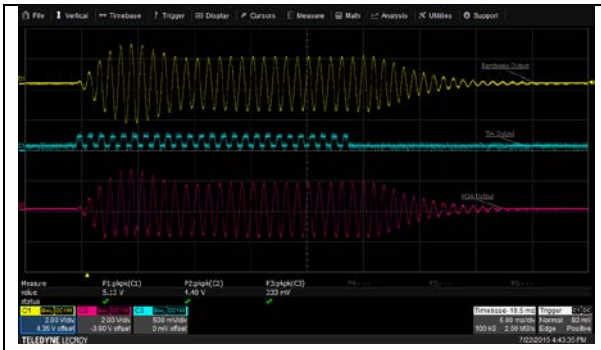

Distance = 2.5cm

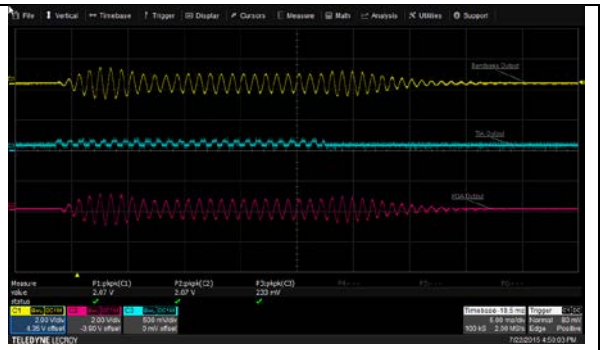

Distance = 3.5cm

Distance = 4.5cm

Distance = 5.5cm

Distance = 6.5cm

Distance = 7.5cm

Distance = 9.5cm

Distance = 11.5cm

Distance = 13.5cm

Distance = 15.5cm

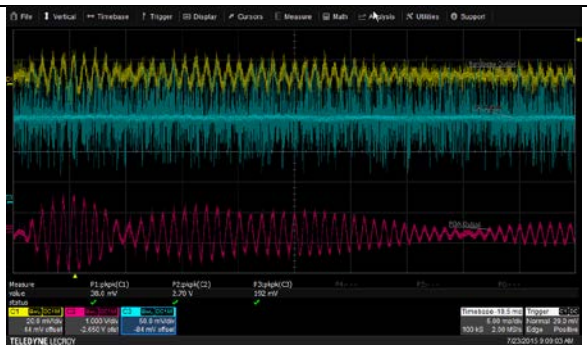

Distance = 20.5cm

Figure 30: Oscilloscope Captures

The data shown in the oscilloscope captures shows that as the target is moved farther away, the signal becomes weaker to the point where the oscilloscope cannot accurately discern the TIA signal over the noise despite being on 50mV/div reference scale. From the PGA data in the above figure (Figure 30), the peak-to-peak value of the signal is measured using onboard measurement tools. This data and the sampled data is used to construct the plot in the following figure (Figure 31). Figure 31 is a plot of the amplitude of the signal measured in hardware versus software's interpretation of the value all as a function of the distance.

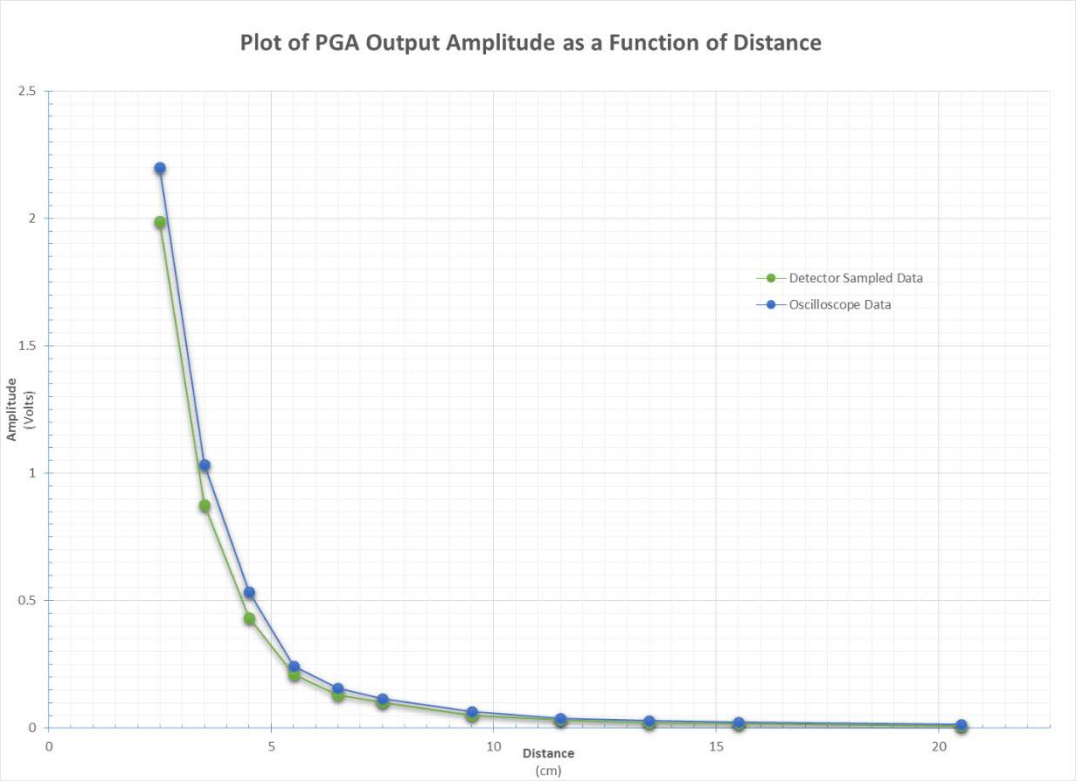

Figure 31: Hardware vs. Software Data Verification

The data in the plot above suggests a high level of correlation between the software and hardware data (hardware data is in blue and the software data is in green). From the plot it can be seen that as the distance is increased, the amplitude of the signal decreases similar to the inverse square of the distance. The error between the two signals is most probable to have been caused by a misalignment in the capture times in the data between the oscilloscope and the actual device; meaning, that the data points used to calculate the peak-to-peak measurements on the oscilloscope and are different than what is sampled by the device. To account for this in testing, an external trigger could be setup to indicate to the oscilloscope when to capture the data based on when the

device is sampling the data. Doing this would most certainly reduce error in the measurement but require changes in the code to toggle an unused GPIO pin on the microprocessor.

3.2 PH MEASUREMENT TEST

The purpose of this experiment is to show the effectiveness of this sensor with the sensing of pH. The test is setup to use two analog boards and a single digital board. The two analog boards provide the ratiometric fluorescence measurement. The excitation LEDs are selected to have peak illumination of 405nm and 465nm. For the emission side of the detector utilizes a narrow bandpass optical filter with the center wavelength positioned at 525nm. The figure below (Figure 32) shows the test measurement setup.

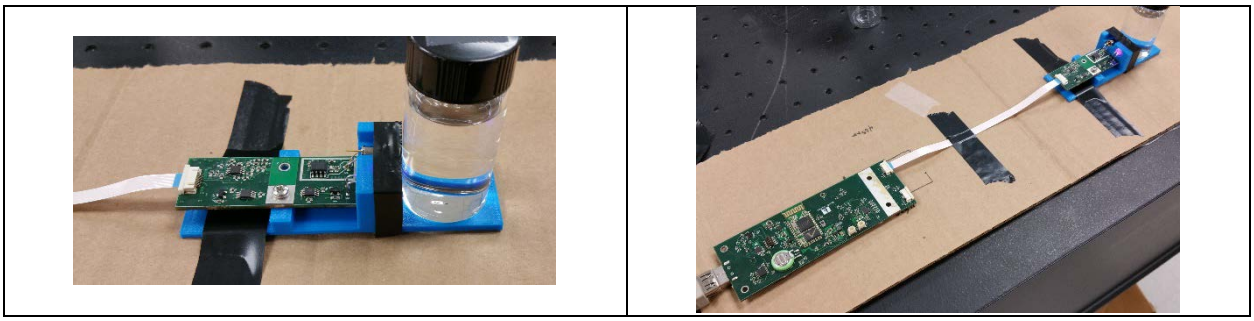

Figure 32: pH Evaluation Test Setup

As can be seen, the test vial and analog board are contained in a single 3-D printed cradle. The test vial is kept close to the sensor head to reduce optical path loss. This setup allowed for more repeatable measurements.

For this test, there are a total of 10 different solutions with pH values ranging from 1 to 7. A reference measuring device (Oakton pH6+ Meter) is used to verify the pH level of each sample. Table 4, below, indicates the pH level recorded for each sample using the reference meter.

Table 4: Refence pH Measurments for each Test Sample

Sample #	Measured pH (reference)
1	1.31
2	1.73
3	2.15
4	2.85
5	3.88
6	5.2
7	6.16
8	6.24
9	6.59
10	7.33

The reference device is accurate to 0.01 pH units and a local calibration is performed on the device using pH solutions of 4.01, 7 and 11.01. Each of the test samples is then tested using the fluorescence meter described in this paper. The testing of this device is done serially, in this case referring to the fact that each of the test samples are tested using the 405nm excitation analog board and then retested using the 465nm board. Simultaneous measurements were not completed for this test since a test jig to house both analog boards and the test sample was not designed. In any case, this test method provides proof of concept and performance. Further commercialization of the product would be required to incorporate two sensors onto a single sensing platform. The following table (Table 5) represents the output voltage recorded using each analog board and the subsequent ratio of the two readings.

Table 5: Ratiometric Fluorescence Measurements

Sample #	405nm Excitation LED (Volts)	465nm Excitation LED (Volts)	465nm / 405nm LED Ratio
1	0.299919	1.921155	0.156114
2	0.288209	1.93526	0.148925
3	0.272612	1.894212	0.143918
4	0.264646	1.926306	0.137385
5	0.253038	1.901104	0.133101
6	0.265181	1.950970	0.135923
7	0.256989	1.929182	0.133211
8	0.248897	1.951273	0.127556
9	0.275038	1.949913	0.141051
10	0.310484	1.940004	0.160043

This ratio column is plotted as a function of measured pH and can be seen in the next figure (Figure 33). The data is linear (boxed in red) assuming the pH of the substance is in the acid region. The figure below (Figure 33) correlates the ratiometric readings acquired from all of the test samples tested.

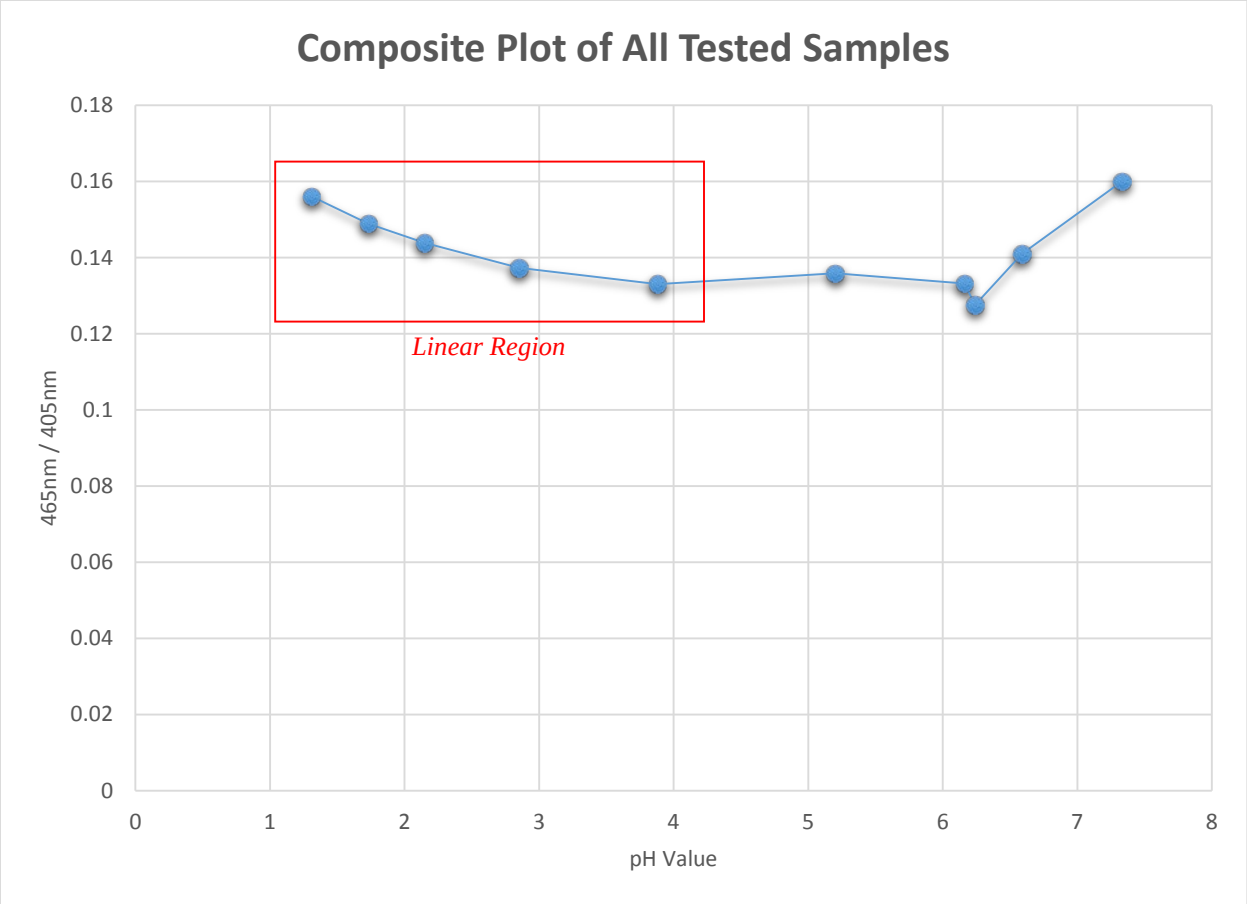

Figure 33: Scatter Plot of Ratiometric Data Collected for all pH Samples Tested

The following figure (Figure 34) zooms in on the region boxed in red in the above figure (Figure 33). From this data a linear relationship can be made and using a linear regression, a formula is constructed that maps the obtained ratio from the measurement to the pH value of the solution. This equation is known as the linear calibration curve and provides reasonable mapping of the measured ratio to the pH value.

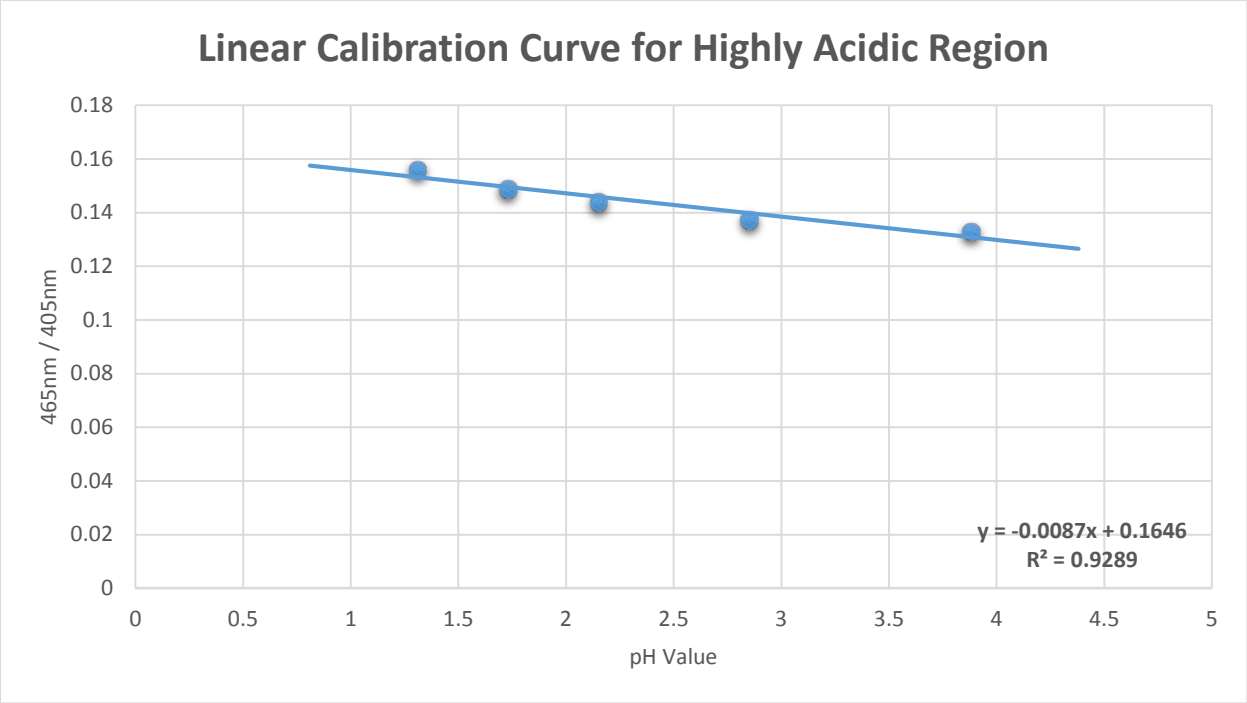

Figure 34: Linear Calibration Curve for the Highly Acidic Region

The following equation is derived from the linear regression obtained from the raw test data. This equation can be used to translate a measured ratio into a corresponding pH value so long as the pH value of the sample is in the acidic region.

$$pH = -\frac{(ratio - 0.1646)}{0.0087} \qquad \text{Eq. 1}$$

A couple things to note about the performance and testing of the device are that the position of the test vial in the cradle is critical. Additionally, the test results for each test sample were greatly affected by which portion of the glass test vial was facing the sensor. To reduce the number of contributing variables to the variability of the measurement, a single vial was used and a position was marked on the vial and the cradle. A test solution was poured into the vial and positioned in the same relative position. One thing to note is that even taking the time to align the mark on the vial and the cradle up there is still variability in the alignment and this also affected the measurement; granted, less error was introduced by performing the test in this manner.

The following table (Table 6) uses the proposed linear equation (Eq. 1) to determine the error of pH measured by the device compared to the reference pH meter used.

Table 6: Estimated Measurement Error

Sample #	Measured pH Value *(Reference Device)*	Estimated pH Value *(Designed Device)*	Error
1	1.31	0.975	26%
2	1.73	1.801	4%
3	2.15	2.377	11%
4	2.85	3.128	10%
5	3.88	3.620	7%
6	5.2	3.296	37%
7	6.16	3.607	41%
8	6.24	4.257	32%
9	6.59	2.706	59%
10	7.33	0.523	93%

From the data above, the error in the measurement increases as the pH of the solution becomes more neutral. The equation derived from the test data is only applicable in the highly acid region and as the table above shows introduces significant error.

4.0 SUMMARY

Overall the device electrically worked great but was not able to perform as accurate of pH readings as intended. Unfortunately, the device seemed to suffer from some test setup conditions that were not able to be corrected or accounted for. Based on the two tests performed on the device, the device performs reasonably well but does have some susceptibilities.

For the electrical signal integrity testing, the device performed extremely well and the overall software versus hardware results were highly correlated. Also, the device also shows that it is highly sensitive based on the devices ability to discern extremely low signals into verifiable results.

As for the pH testing experiment, the results obtained did not yield as accurate results as originally intended. Unfortunately, the test setup was highly susceptible to configuration of the test vial. Also, the repeatability of measurements was also highly variable based on the test setup. Furthermore, the 3-D printed part was extremely porous and allowed for light to bleed over into the sensing chamber behind the emission filter. This issue was mitigated through the use of black electrical tape which helped to provide the needed optical isolation between the two chambers on the device. A positive outcome is that the device was able to perform and detect various levels of pH without the aid of any fluorescent dye. The test relied solely on the properties of the solution (in this case the various concentrations of the HCL and DI water) used. If a dye was used in combination with a better test jig, the results obtained would likely provide more accurate and consistent measurements.

5.0 FUTURE WORK

Additional work to shrink the overall size of the product and reduce the overall component count but still maintain the performance is highly desired. The major cost considerations on the design deal with the high-cost associated with the precision components and the optical filters.

To enhance the capability of the device the current processor (Atmel based 8-bit) can be update to an ARM-M4 core to perform floating point math and to provide additional processing power. Currently, all data conversion is completed off the board with supplemental PC software application written using LabVIEW. Ideally, the microprocessor could perform all the complex math and report the data directly to the user with no need to perform any conversion. Furthermore, going with an ARM processor the flash memory density and RAM density is significantly higher allowing for the ability to create more complex program and the ability to do additional sensing if needed.

To increase the overall performance and reduce the measurement error, a better test fixture jig would need to be created that would allow for simultaneous measurements and that would optically isolate the two chambers better. Furthermore, adding the influence of a ratiometric dye to the solution would greatly enhance the devices performance and would allow it to more accurately predict the pH value of a given solution.

REFERENCES

[1] C. Y. Dong and P. T. So, Fluorescence Spectrophotometry, John Wiley & Sons, Ltd, 2002. © 2013 Wiley-VCH Verlag GmbH & Co. KGaA, Weinheim

[2] Reproduced with permission from [Y. Kostov and G. Rao, "Low-Cost Device for Ratiometric Fluorecence Measurements," *Reivew of Scientific Instruments,* vol. 70, no. 12, pp. 4466-4470, December 1999]. Copyright 1999. AIP Publishing LLC. http://dx.doi.org/10.1063/1.1150098

[3] X. Ge, Y. Kostov, R. Henderson, N. Selock and G. Rao, "A Low-Cost Fluorescent Sensor for pCO2 Measurments," *Chemosensors,* pp. 108-120, 2014.

[4] "Freescale Smiconductor Application Note High Speed Layout Deisgn Guidelines AN2536," 2006. [Online]. Available: http://cache.freescale.com/files/32bit/doc/app_note/AN2536.pdf.